Methodology to minimize the dynamic response of tall buildings under wind load controlled through semi-active magneto-rheological dampers

Alex Koch de Almeida, Francisco da Silva Brandão
Federal University of Rio Grande do Sul (UFRGS), Brazil.
alex.almeida@ufrgs.br, https://orcid.org/0000-0001-9923-3434
eng.fsbrandao@gmail.com, https://orcid.org/0000-0001-7888-6321

Letícia Fleck Fadel Miguel
Department of Mechanical Engineering (DEMEC), Federal University of Rio Grande do Sul (UFRGS), Brazil.
letffm@ufrgs.br, https://orcid.org/0000-0001-9165-4306

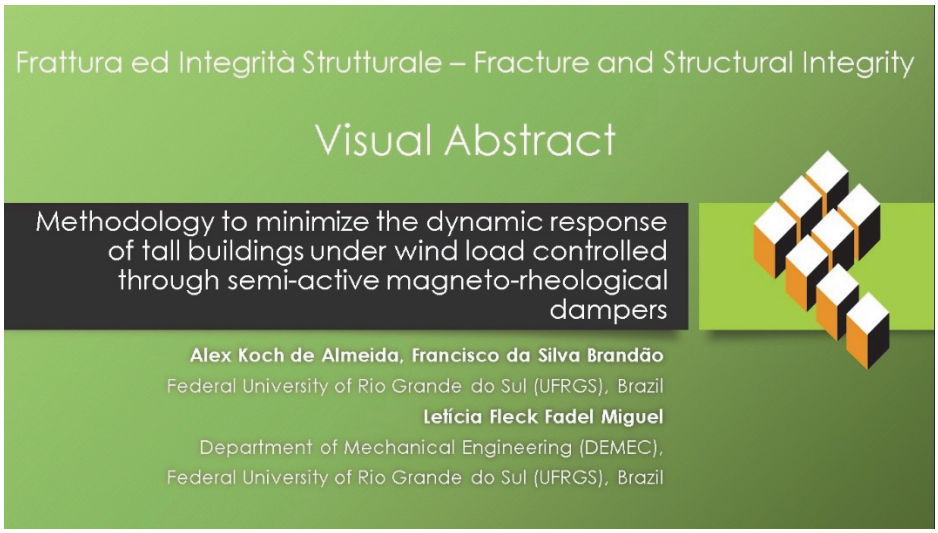

Citation: Almeida, A. K., Brandão, F. S., Miguel, L. F. F., Methodology to minimize the dynamic response of tall buildings under wind load controlled through semi-active magneto-rheological dampers, Frattura ed Integrità Strutturale, 69 (2024) 89-105.

Received: 26.01.2024
Accepted: 15.04.2021
Published: 25.04.2024
Issue: 07.2024

KEYWORDS. Vibration Control, MR dampers, Structural Optimization, Tall Buildings, Wind Load.

INTRODUCTION

The construction of tall buildings has become easier, mainly due to technological advances in materials and construction techniques. Linked to the growth of urban centers, which causes a decrease in free spaces for new constructions, building taller structures has become a necessity. Consequently, buildings are being built increasingly taller and slender, and therefore more vulnerable to wind action [1] Thus, an important area of research is the study of slender structures, such as tall buildings, subject to the dynamic effects of wind. It is essential to design structures that meet comfort and safety requirements at the lowest possible cost. In this context, the area of structural optimization together with the area of vibration control becomes fundamental.

Regarding the area of optimization, both deterministic and stochastic methods can be used [2], with an advantage for stochastic methods when dealing with complex problems such as the one studied in the present work. Several topics are

currently studied in the field of structural mass optimization, for example, studies on minimizing the mass of structures subject to natural frequency constraints [3-7]. Although structural optimization is an effective tool, the combination of this with other tools is often necessary.

Considering this context, the vibration control devices, classified as passive, active, and semi-active can be added to the structures to improve their performance against dynamic actions, and the optimization process can be also implemented to reach the maximum performance of these devices. The passive devices, which have pre-defined properties, are characterized by not using an external power source, while the active ones, which apply force to the structure at the same time as the excitation, need an external power source. The semi-active devices, which have been the object of several recent research, combine the advantages of passive and active devices simultaneously as they have an intrinsic characteristic of adaptability, being able to change their properties with a reduced amount of energy, without applying force to the structure.

Among the semi-active control devices, the Magneto-Rheological (MR) dampers stand out, due to their mechanical simplicity, wide dynamic applicability, low energy cost, great strength, and robustness. These characteristics have shown good adherence to the demands of structural systems in the control of dynamic excitations such as earthquakes and wind [8]. Therefore, civil engineering can take advantage of this type of approach, creating structures able to monitor and control their response under dynamic excitations.

Several studies have been published demonstrating the application of MR dampers in the control of dynamic responses. Among the first experimental studies with prototypes, there are those in which the authors developed experiments with structures of up to 6 degrees of freedom excited at the base in order to simulate an earthquake [9-11]. There are also numerical studies with simple structural models in which the authors developed simulations with structures of up to 20 degrees of freedom excited by earthquakes [12-15], and a study in which the authors developed simulations with a structure of 40 degrees of freedom excited by the wind [16]. It is also worth mentioning the more complex numerical models, such as the one in which the authors studied a structural model called mega-sub-controlled structure excited by wind [17] and the one in which the authors performed a simulation with a 2D frame excited by earthquakes [18]. Hybrid strategies using MR dampers and other types of devices are also being researched, for example in [19]. Finally, considering the theoretical-experimental studies, there is a study in which the authors reported an experiment that was carried out on the cable-stayed Dongting Lake Bridge in China, severely excited by strong winds and rain [20], and the one in which the author analyzed several different structures, considering numerical models with multiple degrees of freedom excited by earthquakes [21].

As highlighted, most of these studies focus on analyzing simplified structural models subjected to earthquakes and, therefore, there is a lack of studies with more complex structural models, able to provide a better description of the behavior of tall buildings subjected to wind excitation. Additionally, unlike most works in the literature, this paper proposes a methodology in which not only the installation of dampers is considered as a way of minimizing vibration amplitudes, but also the optimization of the structure is carried out, with the objective of increasing the fundamental frequency of the building, taking it to values further away from the frequency content of the wind spectrum, and thus reducing the dynamic response. That is, the proposed methodology combines structural optimization with semi-active control devices. Besides, most of the works that propose different types of vibration control systems, for different types of structures and excitations, are related to passive systems, for example [22-42, among others].

Thus, to contribute to filling these gaps, this study focuses on analyzing a tall building, described by a 2D frame model of multiple degrees of freedom, under dynamic wind loading and controlled by semi-active MR dampers. For this, the dynamic responses of three different configurations of the building, under wind excitation, are analyzed, and compared with performance criteria indicated in [43] and [44]. The first configuration, called Original Uncontrolled (C1), consists of a frame building extracted from a tall building originally proposed and analyzed in [45]. The second, called Optimized Uncontrolled (C2), consists of a structure whose fundamental frequency was optimized, via the PSO algorithm, as a function of its mass, from the C1 configuration. The complete procedure for this optimization was presented by the authors in a previous paper [46]. The third and last one, called Optimized Controlled (C3), consists of the C2 configuration controlled through a set of semi-active MR dampers.

PROBLEM FORMULATION AND PROPOSED METHODOLOGY

Structural modelling

The numerical modelling of the structure is approached through the finite element method, considering a 2D frame model, according to the procedures from [47]. The damping matrix, C , was generated using the Rayleigh method, formulated as a linear combination of the global mass matrix, M , and global stiffness matrix, K .

Wind modeling

For the proposed problem, the procedures described in [48] are followed and, therefore, it deals only with synoptic winds (more complex models can be found in [49]). Thus, the wind load is given by:

$$F_D = \overline{F_D} + \widetilde{F_D} \tag{1}$$

in which $\overline{F_D}$ is the mean component and $\widetilde{F_D}$ is the fluctuating component of the drag force, F_D. The mean component of the drag force can be obtained by:

$$\overline{F_D} = \overline{q_0} C_D A_i b^2 \left(z_i / z_r\right)^{2p} \tag{2}$$

in which C_D indicates the drag coefficient that depends on the building shape, A_i is the effective area of exposure considered, orthogonal to the wind direction, b and p are meteorological parameters, z_r is the reference height (10 meters), z_i is the height under analysis and $\overline{q_0}$ is the reference dynamic pressure of the wind, relative to the mean component, given by:

$$\overline{q_0} = \frac{1}{2} \rho_a \overline{V_p}^2 \tag{3}$$

in which ρ_a represents the specific mass of the air (equal to 1.225 kg/m³ at 15 °C and 1013 mbar) and $\overline{V_p}$ is the design wind velocity, expressed by:

$$\overline{V_p} = 0.69 V_0 S_1 S_3 \tag{4}$$

in which V_0 is the base wind velocity, S_1 is the topographic correction factor and S_3 is the statistical correction factor. The fluctuating component of the drag force can be obtained by:

$$\widetilde{F_D} = \widetilde{q_0} C_D A_i \tag{5}$$

in which $\widetilde{q_0}$ is the reference dynamic pressure of the wind, relative to the fluctuating component, given by:

$$\widetilde{q_0} = \frac{1}{2} \rho_a 2\overline{V_p} b \left(z_i / z_r\right)^p \Delta v \tag{6}$$

in which $\Delta v\left(c_x, c_y, t\right)$ is the fluctuating component of the wind velocity, c_x and c_y are the horizontal and vertical coordinates, respectively, in a Cartesian plane, of the point under analysis, and t is the time. The fluctuating component of wind velocity is considered a normal random process with zero mean. The problem was formulated through the superposition of harmonic waves, in a process known as the spectral representation method [50]. Using this method, it is possible to convert the energy described by the spectrum in the frequency domain to the time domain and this implies the inclusion of a random component in the process, as shown in:

$$\Delta V_s(t) = \sum_{i=1}^{n_f} \sqrt{2 S_i\left(f_i\right) \Delta f_i} \cos\left(2\pi f_i t + \Phi_i\right) \tag{7}$$

in which $\Delta V_s(t)$ is a fluctuating velocity signal at a given position in space, with $s = \{1,2,3,4\}$, S_i is the spectral density of the wind velocity, f_i is the frequencies considered, n_f is the maximum value of the considered frequency range, Δf_i is

the frequency increment and Φ_i is the phase angle which is a random variable with a uniform probability distribution function between 0 and 2π.Among the available spectral models, the one proposed by Davenport is used, according to [51], described by:

$$\frac{f_i S_i(f_i)}{u_*^2} = \frac{4n_*^2}{\left(1+n_*^2\right)^{4/3}} \quad ; \quad u_* = \frac{k_* \bar{V}_{10}}{\ln\left(\frac{z_{ref}}{z_0}\right)} \quad ; \quad n_* = \frac{f_i L_*}{\bar{V}_{10}} \tag{8}$$

in which u_* is the friction velocity, n_* is the dimensionless frequency, k_* represents the Kármán constant, $\bar{V}_{10}$ is the mean wind velocity at 10 meters above ground level, z_{ref} is the reference height, z_o is the roughness length and L_* is a fitting constant of the spectral model. In order to consider the spatial correlation among the signals of fluctuating velocity, the fluctuating component of the wind velocity is determined, according to [52] as a result of the approach proposed in [53], through:

$$\begin{aligned}\Delta V(c_x, c_y, t) = \Delta V_1(t) + \frac{\Delta V_2(t) - \Delta V_1(t)}{c_a} c_x + \frac{\Delta V_3(t) - \Delta V_1(t)}{c_b} c_y + \\ + \frac{\Delta V_4(t) - \Delta V_3(t) - \Delta V_2(t) + \Delta V_1(t)}{c_a c_b} c_x c_y\end{aligned} \tag{9}$$

Eqn. (9) determines the fluctuating velocity at a given point of interest from horizontal and vertical coordinates, c_x and c_y, respectively, in a Cartesian plane, where the s fluctuating velocity signals are spaced by a horizontal correlation length c_a and by a vertical correlation length c_b. Therefore, the frame under study is inserted perpendicularly into the correlation plane, and the fluctuating velocity is determined at each of the external nodes of the structure. c_a and c_b are determined through Eqn. (10) proposed in [52] as a result of linear regression applied to experimental data from [51], where z_c is the structure height.

$$\begin{aligned} c_a &= 1.60 z_c + 22.1 \\ c_b &= 0.93 z_c + 29.3 \end{aligned} \tag{10}$$

MR damper modeling

The semi-active control system usually is originated from passive control systems that are modified to allow adjustment of mechanical properties, for example, devices that dissipate energy through modified viscous fluids to behave in a semi-active configuration. On the one hand, as in an active control system, sensors installed in the structure monitor the response, and a controller, based on the response, generates an appropriate command signal for the device. On the other hand, as in a passive control system, the control forces are developed as a result of the movement of the structure itself [54], that is, semi-active dampers have mechanical properties or parameters that can be adjusted to improve their performance as an active control system, maintaining the reliability of passive control systems [55]. Among the semi-active control devices, the controllable fluid dampers stand out, employing fluids in their interior that can adjust their mechanical properties quickly in reaction to external forces. Among the applicable fluids, the magneto-rheological (MR), like the model shown in Fig. 1, has as an essential feature its ability to reversibly change from a free-flowing linear viscous fluid to a semi-solid with a controllable flow force, in milliseconds, when exposed to a magnetic field [56].

MR dampers consist of a cylinder that contains the MR fluid, manipulated through a diaphragm and excited by a coil responsible for transmitting the magnetic signal that changes its properties. The reactive force is transmitted by the Only moving part, the piston. Fig. 1 shows the schematic of the components of an MR damper.

These devices are simple to operate and maintain, have high reliability, and are stable over a wide temperature range. Since they are basically adaptive passive devices, even in case of a malfunction of their semi-active property, the controller in the passive configuration can still contribute to mitigating the effects of dynamic actions. Furthermore, given their high strength,

they are capable of being applied to civil structures using a small energy supply. Under these conditions, MR dampers are promising devices for application in structures subjected to dynamic wind actions. Many rheological models have been developed to describe the behavior of these devices. In this study, the model proposed by Bouc-Wen and adjusted by [55], named modified Bouc-Wen, is used, as shown in Fig. 2.

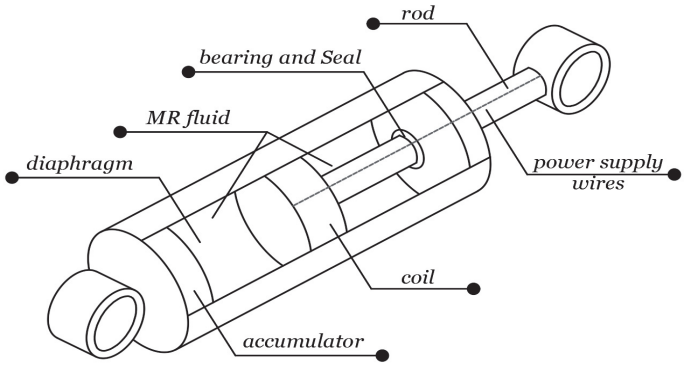

Figure 1: Schematic of the components of an MR damper.

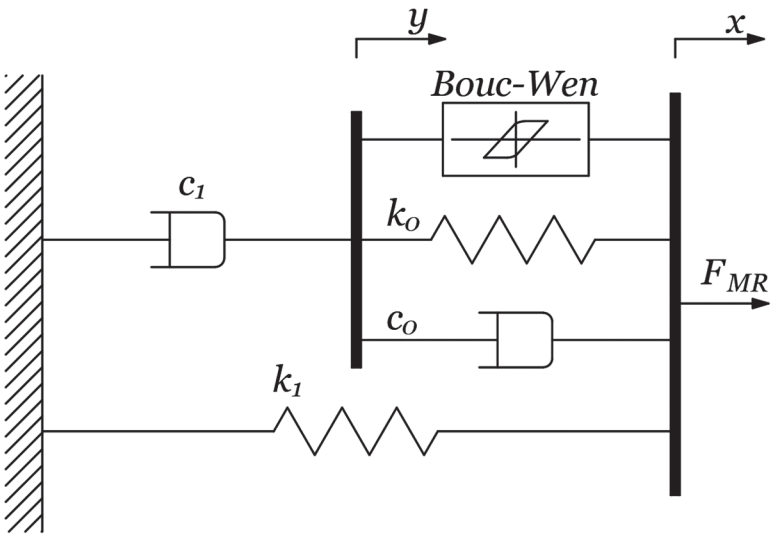

Figure 2: Modified Bouc-Wen rheological model.

This model is governed by:

$$F_{MR} = c_1 \dot{y} + k_1 \left(x - x_0 \right) \tag{11}$$

$$\dot{y} = \frac{1}{c_0 + c_1} \left[\alpha z + c_0 \dot{x} + k_0 \left(x - y \right) \right] \tag{12}$$

$$\dot{z} = -\beta \left| \dot{x} - \dot{y} \right| z \left| z \right|^{n_{bw}-1} - \gamma \left(\dot{x} - \dot{y} \right) \left| z \right|^{n_{bw}} + A_{bw} \left(\dot{x} - \dot{y} \right) \tag{13}$$

in which $F_{MR}(t)$ is the total reactive force generated by the system, c_0 is the viscous damping observed at higher velocities, k_0 is present to control stiffness at higher velocities, c_1 is a damping included in the model to produce the roll-off effect observed at low velocities, k_1 is the stiffness of the accumulator, x and y are the displacements of the damper, z is the evolutionary variable, x_0 is the initial displacement of the spring k_1 associated with the nominal force of the accumulator. α, β, γ, A_{bw} e n_{bw} are parameters that describe the hysteresis of the system. The model parameters that are used in this

work were experimentally determined by [21] for the MR RD-1005-3 damper (Lord corporation) and are presented in Tab. 1, where I is the electrical current supplied to the device, whose maximum value, associated with the saturation of the magnetic field, is 0.5 A.

Independent parameters	$A_{bw}[-]$	$\beta\left[\text{mm}^{-1}\right]$	$\gamma\left[\text{mm}^{-1}\right]$	$k_0[N/mm]$	$k_1(x-x_0)[\text{N}]$	n_{bw}
	10.013	3.044	0.103	1.121	40	2
Current dependent parameters	$\alpha(\text{I}) = -826.67\text{I}^3 + 905.14\text{I}^2 + 412.52\text{I} + 38.24\,[\text{N}]$					
	$c_0(\text{I}) = -11.73\text{I}^3 + 10.51\text{I}^2 + 11.02\text{I} + 0.59\,[\text{N.s/mm}]$					
	$c_1(\text{I}) = -54.40\text{I}^3 + 57.03\text{I}^2 + 64.57\text{I} + 4.73\,[\text{N.s/mm}]$					

Table 1: Parameters of the modified Bouc-Wen model for the MR RD-1005-3 damper [21].

The MR damper RD-1005-3 is used for low force capacity applications, such as industrial suspensions. It can be verified in its specifications that its peak force in response to a current value of 1 A is 2,224 kN [21]. Knowing this, the total reactive force of the equipment (F_{MR}) will be multiplied by an amplification factor (Ω). This adjustment represents Ω dampers acting in parallel on each m controlled mass, in order to simulate a robust device compatible with the drag force.

Equation of motion

The numerical modeling of the system considering the damping forces of the MR dampers was approached according to [57], in this way, the matrix representation of the dynamic equilibrium equation is:

$$M\ddot{\vec{x}} + C\dot{\vec{x}} + K\vec{x} = \vec{F} - \Omega\vec{F}_{MR} \tag{14}$$

in which $\vec{x}$, $\dot{\vec{x}}$, and $\ddot{\vec{x}}$ are the displacement, velocity, and acceleration vectors, respectively. $\vec{F}$ is the external forces vector and $\vec{F}_{MR}$ is the damping forces vector, both applied at the indicated degrees of freedom. To solve Eqn. (14) in the time domain the Newmark method associated with the Runge-Kutta (RK4) is applied. For C3, the dynamic equilibrium equation is solved repeatedly, gradually increasing the amplification factor Ω until satisfying the performance criterion, according to the pseudocode shown in Fig. 3.

Set initial value $\Omega(0) = 10$;
repeat
  Solving the Dynamic Equilibrium Equation
  $M\ddot{\vec{x}} + C\dot{\vec{x}} + K\vec{x} = \vec{F} - \Omega\vec{F}_{MR}$
  if not meet the performance criteria **then**
  $\Omega(i+1) = \Omega(i) + 10$
until meet the performance criteria;

Figure 3: Pseudocode for defining the amplification factor.

LQR-CO control strategy

Active structural control research efforts have focused on a variety of control techniques based on several design criteria. Some are considered classic, as they are direct applications of modern control theory, among them is the optimal control technique [58]. As highlighted in [59], the optimal controller problem can be defined as the determination of a control law for a given system in order to reach a specific optimal criterion by minimizing a pre-defined performance index. Among the strategies associated with optimal control, there is the so-called clipped optimal (CO), developed in [9], which, according to [60], is the most successful strategy so far for the control of systems that use controllable fluid devices. In this case, a

controller is designed based on linear control strategies, such as the Linear Quadratic Regulator (LQR), for example, as if the control device were active. However, a decision block for the current applied to the actuator and measuring the actuating control force are integrated into the system to properly adjust the control command and accommodate dissipative characteristics and non-linearities in device behavior. The LQR, widely studied and widespread, can be established as a control engineering tool that aims to determine an ideal control by minimizing a quadratic performance index when the control is a linear function of the response [58, 59, and 61].

To take advantage of the semi-active behavior of MR dampers, the LQR controller associated with the Clipped Optimal (LQR-CO) strategy is used. Fig. 4 shows the block diagram of this strategy.

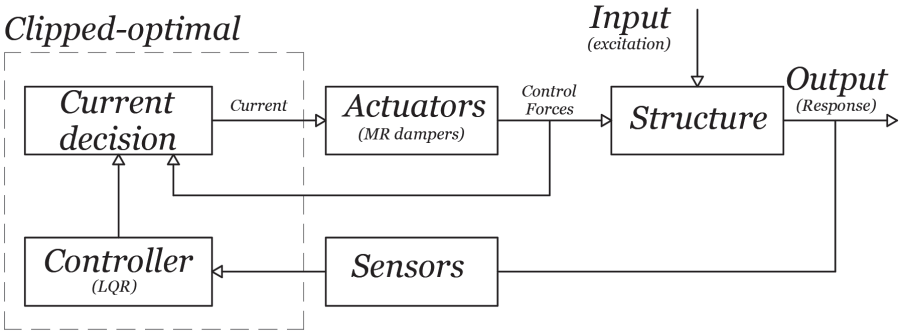

Figure 4: LQR-CO Block Diagram.

The LQR-CO strategy works through the cycle shown in Fig. 4, as follows:

- The structure is excited by an external force (input);
- The structure reacts to the excitation and presents a response (output), in terms of displacement, velocity, and acceleration;
- The response is captured by sensors installed in the structure (or in numerical simulation it is obtained by integration) that take this information to the controller;
- Based on the response, the LQR controller determines an optimal control force and sends this information to the current decision block;
- The current decision block compares the actuating control forces with those determined by the controller and then decides the current to be applied to the actuators in order to position the system control forces as close as possible to the optimal forces defined by the controller;
- Since actuators have their properties controlled by the current, a new current produces new control forces that are applied to the structure.

The optimal control force at each instant of time can be determined by Eqn. (15), approached by [58, 59, and 61].

$$\vec{f}_0(t) = -\frac{1}{2} R^{-1} B^T P \vec{e}(t) \tag{15}$$

$$PA - \frac{1}{2} PBR^{-1}B^T + A^T P + 2Q = 0 \tag{16}$$

$$A = \begin{bmatrix} 0_{(n,n)} & Id_{(n,n)} \\ -M^{-1}K & -M^{-1}C \end{bmatrix} \tag{17}$$

$$B = \begin{bmatrix} 0_{(n,n)} \\ -M^{-1}\Gamma_{(n,m)} \end{bmatrix} \tag{18}$$

$$\vec{e}(t) = \begin{bmatrix} x_n(t) \\ \dot{x}_n(t) \end{bmatrix} \tag{19}$$

in which $\overrightarrow{f_o}(t)$ is the vector of optimal forces at each instant of time, with the m optimal forces f_o and n control forces applied to the system. $\vec{e}(t)$ is the state vector of the system composed of the n displacements, $x(t)$, and the n velocities, $\dot{x}(t)$, and finally, n is the number of degrees of freedom of the system. B is the matrix that describes the control forces in the state space, Γ is the matrix that describes the location of the m control forces. Q and R are called weighting matrices, high values for elements of Q mean prioritizing the reduction of the response over control forces, and high values for elements of R mean the opposite; in general, these values are obtained in a testing process aiming at the best result. A is the system state matrix and Id is the identity matrix. P is the Riccati matrix. Once the vector $\overrightarrow{f_o}(t)$ is determined, the selection of the current to be applied to the damper can be obtained, according to [9], by:

$$I = I_{max} H\left[\left(f_o - F_{mr}\right) F_{mr}\right] \tag{20}$$

in which I_{max} is the maximum current associated with the saturation of the magnetic field and $H(-)$ is the Heaviside function. In this way, the damper force is controlled indirectly, through current control, that is, when the damper is providing the optimal force, the applied current remains unchanged, if the magnitude of the force produced by the damper is less than the magnitude of the desired optimum force and both forces have the same sign, the applied current is increased to the maximum level.

Performance criteria

Three different performance criteria, related to the Serviceability Limit State, are considered in this paper. The first, indicated in Appendix CC of [43], refers to the maximum permissible horizontal displacement of the building (D_{max}), determined through Eqn. (21), in which H_t is the total height of the building.

$$D_{max} = \frac{H_t}{600} \tag{21}$$

The second indicates the maximum permissible displacement between adjacent floors (story drift). According to the American standard [43], the story drift (SD) cannot exceed approximately 1 cm, in this case $SD_{max} \cong 1cm$. Both limits are generally sufficient to minimize damage to the wall covering and non-load-bearing walls [43]. Finally, the third is related to the maximum permissible acceleration ($\text{Acc}_{\max}$). According to [43], continuous vibrations (over a period of minutes) with an acceleration of the order of $0.005g$ to $0.01g$, in which g is the acceleration due to gravity, are uncomfortable for most people. Tab. 2 presents the acceleration limits related to user sensitivity from [44].

Perception	$\text{Acc}_{\max}$
Imperceptible	$< 0.005\ g$
Noticeable	$0.005\ g$ to $0.015\ g$
Uncomfortable	$0.015\ g$ to $0.05\ g$
Very uncomfortable	$0.05\ g$ to $0.15\ g$
Intolerable	$> 0.15\ g$

Table 2: Limit acceleration according to [44].

It is important to note that this is not the main design criterion because, depending on the recurrence time, these accelerations, even if uncomfortable, are acceptable [44]. Thus, considering the previous information, $\text{Acc}_{\max} = 0.01g$ is adopted as the limiting criterion, thus allowing accelerations within the noticeable sensitivity range.

RESULTS AND DISCUSSIONS

Analyzed structures

Three different structural configurations are analyzed in this study. The first, C1, is characterized by a 2D frame extracted from a building previously proposed and analyzed by [45] designed as a reinforced concrete structure with fck equal to 50 MPa, symmetrical and with dimensions in plan of 15m × 15m, 35 floors, 99.75m high, 2.85m high between slabs and 12cm thick on each slab. The building analyzed in this work is considered fixed at the foundation and composed of rectangular columns on the sides, "L" columns in the central part, and continuous rectangular beams discretized in 144 nodes, 245 elements, and 432 degrees of freedom. The details of this frame in its Original Uncontrolled configuration (C1) are shown in Fig. 5. In this configuration, the dimensions of the elements are repeated on all floors.

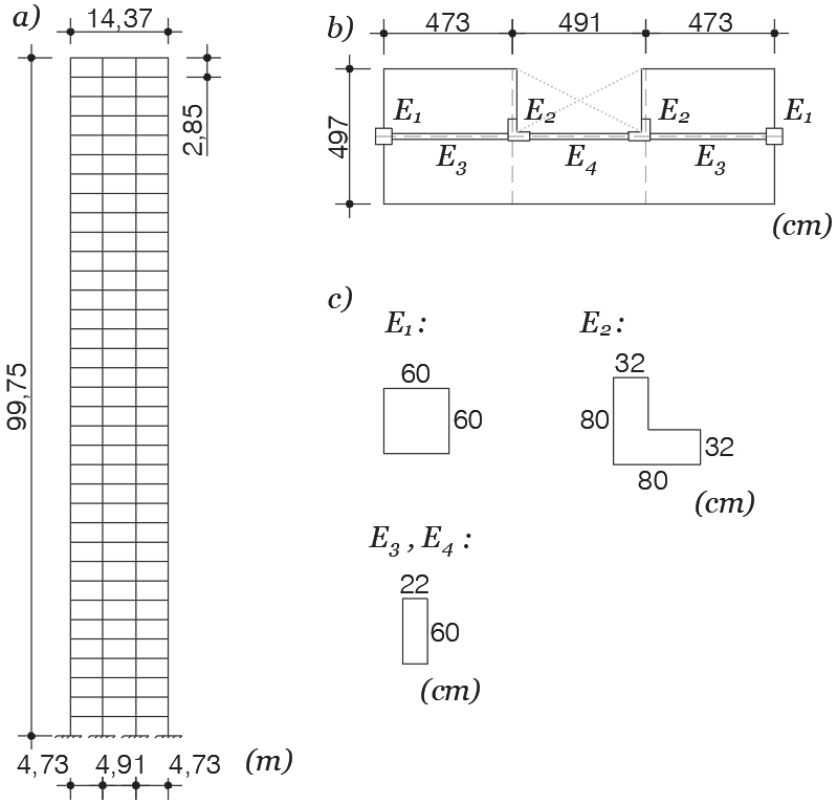

Figure 5: Structure analyzed in uncontrolled original configuration (C1). a) 2D frame, b) Cross section in plan considered, c) Cross section of columns (E1 and E2) and beams (E3 and E4).

At the mass matrix, E and ρ are taken as 3.4 x10^{10} N/m² and 2500 kg/m³, respectively, and concentrated masses of the slabs are considered at the respective nodes of each floor, considering the appropriate influence area. Thus, the structure in its Original Uncontrolled configuration (C1) has a fundamental frequency of 0.34 Hz and a mass of 1171.6 tons.

The second configuration, called Optimized Uncontrolled (C2), consists of the C1 configuration in which the fundamental frequency is optimized, via the PSO algorithm, as a function of its mass. That is, the objective function of the optimization process, which has the maximum mass as a constraint, is to maximize the fundamental frequency of the building, taking it to values further away from the frequency content of the wind spectrum, and thus reducing the dynamic response. This complete optimization procedure was presented by the authors in a previous work [46].

In this scenario, the dimensions of the elements vary depending on their position, and their values can be verified in the authors' previous paper [46]. Thus, the structure in the Optimized Uncontrolled configuration (C2) has a fundamental frequency of 0.50 Hz and a mass of 1526.7 tons, which means an increase of almost 50% (47.06%) in the fundamental frequency against an increase of approximately 30% (30.31%) in the mass of the structure in relation to the C1 configuration.

The third and last one, called Optimized Controlled (C3), presents the C2 configuration with the application of a set of semi-active MR dampers, detailed in the next section.

Vibration control through semi-active MR dampers

In order to obtain the Optimized Controlled configuration (C3), 35 MR dampers are applied to the central frames of the Optimized Uncontrolled structure (C2), one per floor. Each floor is controlled by the damping force F_{MR}^{m}, with $m = \{1\ to\ 35\}$, as illustrated in Fig. 6.

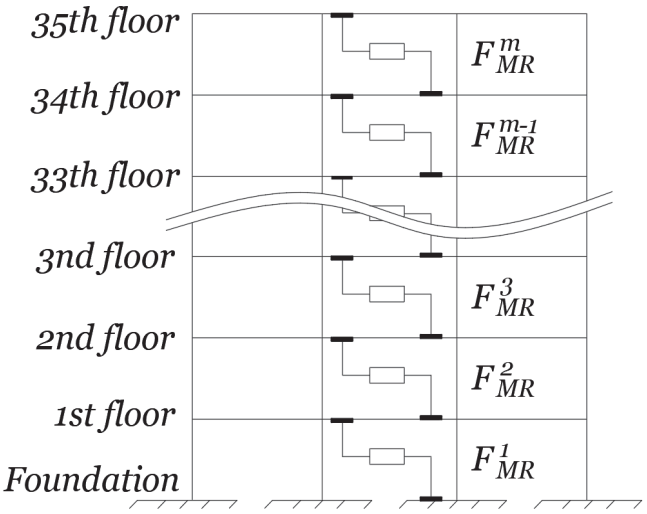

Figure 6: Position of the dampers.

In the LQR solution, the following weight matrices are considered, as indicated by [62]:

$$Q = \begin{bmatrix} K & 0_{(n,n)} \\ 0_{(n,n)} & 0_{(n,n)} \end{bmatrix} \text{ and } R = 10^{-7} I_{d(m,m)} \tag{22}$$

Dynamic wind load

The dynamic wind load is modeled according to the procedures presented previously. Tab. 3 presents a summary of the parameters used, in which S_3 is adopted considering the Serviceability Limit State, with a recurrence time of 10 years.

Parameter	Unity	Value
C_D	-	1.45
A_i	m²	10.69
V_0	m/s	43
S_1	-	1
S_3	-	0.78
b	-	1
p	-	0.15
f_i	Hz	$10^{-5} \sim 10$
k_*	-	0.4
z_{ref}	m	10
z_o	m	0.07
L_*	m	1200

Table 3: Parameters used to determine the wind load.

Fig. 7 shows the drag force at floor 01 (first), floor 20 (approximately half the height of the frame), and floor 35 (last floor).

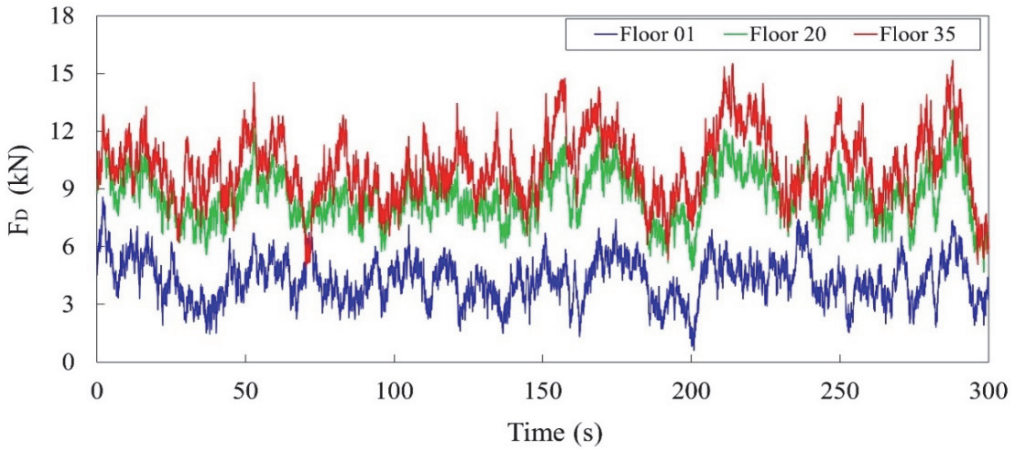

Figure 7: Drag force.

The three configurations, C1, C2, and C3, are horizontally subjected to the dynamic wind action, as shown in Fig. 8, and the dynamic equilibrium equation is solved for each of them. For C3 the amplification factor Ω that satisfied the performance criterion is 660.

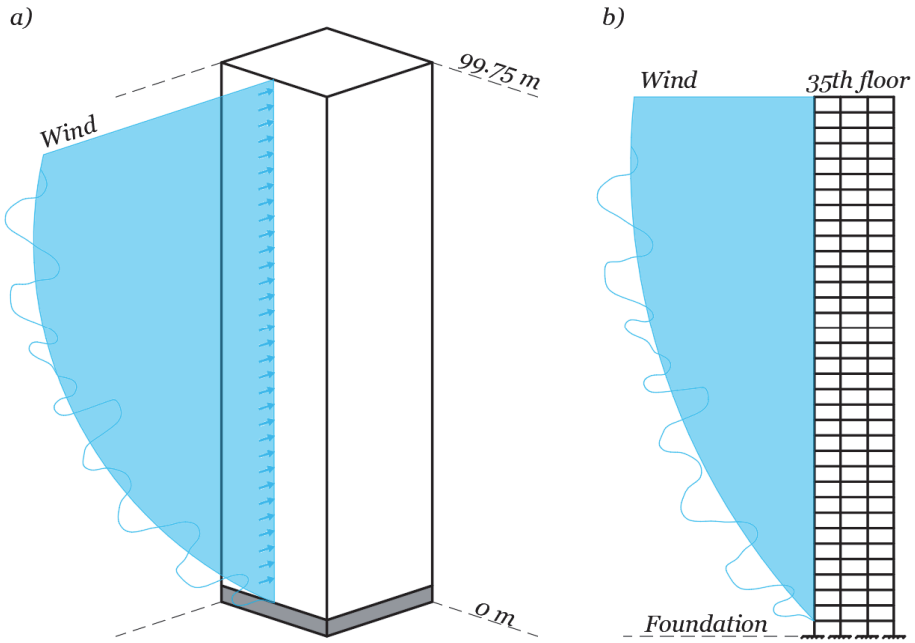

Figure 8: Structure analyzed. a) Perspective, b) 2D frame.

Results of the structural configurations

The first result to be analyzed refers to the optimization process of the structural elements. In this process, from the C1 configuration, the C2 configuration is obtained. It is possible to note an increase of 47.06% in the fundamental frequency at a cost of a 30.31% increase in the total mass of the structure. Next, the analysis of the three configurations C1, C2, and C3, subjected to dynamic wind loading is presented. The analysis is based on observing the response, in terms of displacement, story drift, and acceleration, over time (300s).

The maximum displacement at each floor is shown in Fig. 9(a) and the maximum acceleration at each floor is reported in Fig. 9(b). Analyzing these figures, it can be seen that C3 is the best control scenario and presents considerable response reductions. At the top floor, the displacement is reduced from 16.20cm to 8.45cm considering the C2 configuration, and to 4.66cm, considering the C3 configuration. The maximum accelerations are 40.1cm/s², 41.2cm/s² and 9.36cm/s², in configurations C1, C2, and C3, respectively. The displacement over time at the top floor is shown in Fig. 10 and the acceleration is in Fig. 11. For the maximum story drift in each inter-floor, its representation is shown in Fig. 12, in which the maximum values are: 0.58cm, 0.32cm, and 0.23cm for C1, C2, and C3 configurations, respectively.

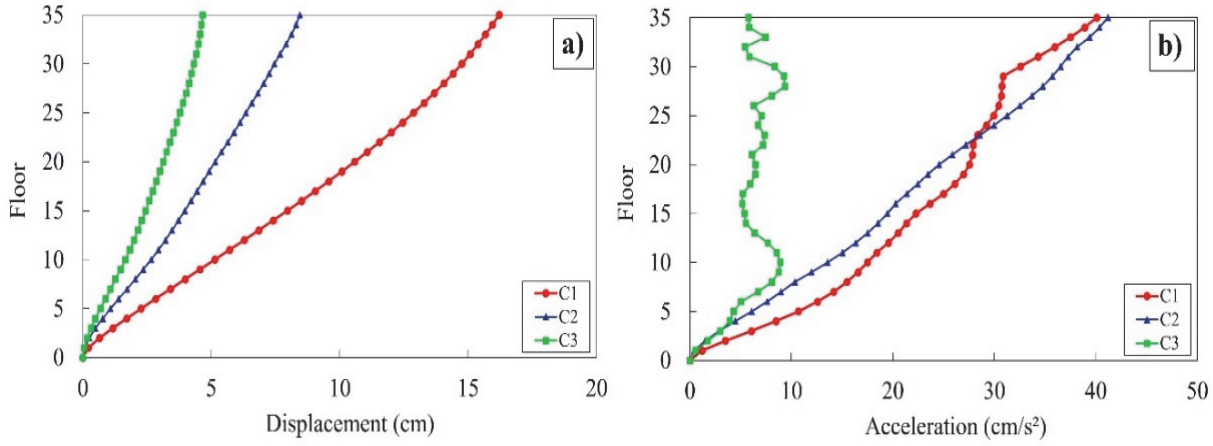

Figure 9: a) Maximum displacements and b) maximum accelerations per floor.

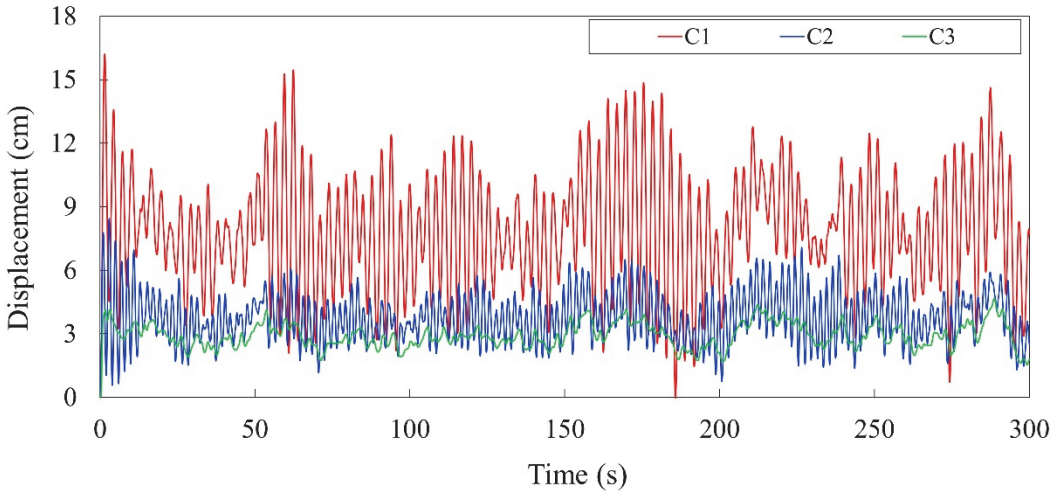

Figure 10: Displacement over time at the top floor.

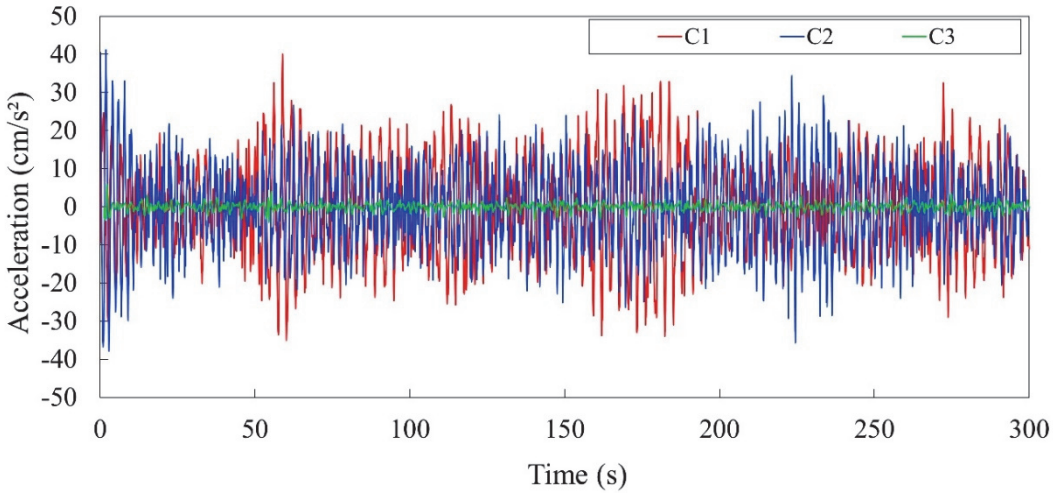

Figure 11: Acceleration over time at the top floor.

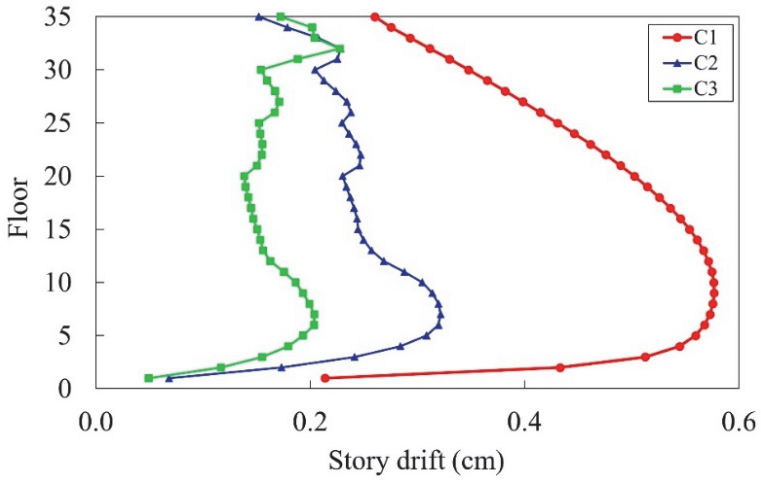

Figure 12: Maximum story drift.

Thus, it could be seen that, in terms of displacements, scenarios C2 and C3 showed a reduction of 47.8% and 71.2%, respectively, in relation to C1, and C3 presented a reduction of 44.85% in relation to C2. For the accelerations, C2 showed an increase of 2.7% and C3 a decrease of 76.7%, respectively, in relation to C1, and C3 reduction of 77.3% in relation to C2. Finally, in terms of story drifts, C2 and C3 showed a reduction of 44.8% and 60.3%, respectively, in relation to C1, and C3 reduction of 28.13% in relation to C2.

For the building under study, the performance criterion related to the maximum horizontal displacement is $D_{max} = 16.6\ cm$. Thus, C1, C2, and C3 met the criterion. Regarding the performance criterion related to maximum story drift, ASCE/SEI 7-16 [43] does not set a value, but indicates an approximation, $SD_{max} \cong 1cm$. In this case, C1, C2, and C3 met the criterion. It is observed, therefore, that the three configurations met the criteria related to maximum horizontal displacement and maximum story drift.

Considering that the maximum acceleration of configuration C3 occurs on the twenty-eighth floor and that this value is -9.36m/s², Fig. 13 shows the acceleration over time, for the C3 on the 28th floor, against the limits presented previously.

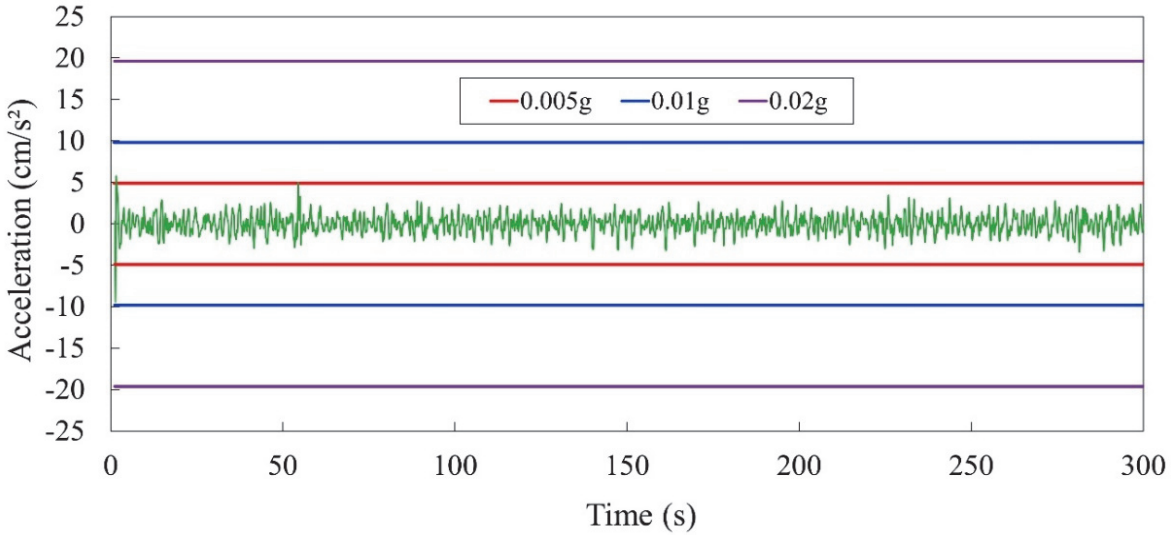

Figure 13: Acceleration over time, C3 on the 28th floor, against performance criterion.

Thus, regarding the performance criterion related to the user's perception, it was verified that on the 28th floor, critical in relation to the acceleration for the C3 configuration, the accelerations were below $0.01g$, that is, the perception is noticeable. Therefore, it can be seen from Figs. 9b), 11, and 13 that only the C3 configuration met the criterion. It is observed, therefore, that in the C3 configuration, the accelerations over time were controlled.

Conclusions

This paper proposed a new methodology to evaluate and optimize the dynamic behavior of tall buildings under wind loading controlled through semi-active Magneto-Rheological dampers. Thus, through this numerical study, it was possible to minimize the dynamic response of a tall building, described through a 2D frame model with multiple degrees of freedom. For this, the responses of three structural configurations (C1, C2, and C3) were evaluated in terms of displacement, story drift, and acceleration, with an evaluation of performance criteria indicated in the literature.

For the maximum displacements at the top floor, it was found that C2 and C3 showed a reduction of 47.8% and 71.2%, respectively, in relation to C1, and C3 reduction of 44.85% in relation to C2. For the maximum story drift, it was verified reductions of 44.8% and 60.3%, to C2 and C3, respectively, in relation to C1 and C3 showed a reduction of 28.13% in relation to C2. Finally, for the maximum accelerations, C2 showed an increase of 2.7% and C3 a decrease of 76.7% in relation to C1, and C3 presented a reduction of 77.3% in relation to C2. Regarding the performance criterion by user's perception, it was found that the 28th floor (critical floor) presented perception noticeable, since the acceleration was below $0.01g$.

From the evaluation of the responses of the three configurations, it was found that the C3 configuration was the only one able to meet all the established performance criteria, and part of this behavior was due to the fundamental frequency optimization and another part was due to the influence of the MR dampers. Thus, the proposed methodology combining structural optimization and MR dampers proved to be a powerful tool for vibration control and it could be used to help designers of this type of structure.

Acknowledgments

The authors acknowledge the financial support of Conselho Nacional de Desenvolvimento Científico e Tecnológico (CNPq) and Coordenação de Aperfeiçoamento de Pessoal de Nível Superior (CAPES), Brazil.

References

[1] Tamura, Y. and Kareem A. (2013). Advanced structural wind engineering, Japan, Springer.

[2] Saka, M.P. and Geem, Z.W. (2013). Mathematical and Metaheuristic Applications in Design Optimization of Steel Frame Structures: An Extensive Review, Mathematical Problems in Engineering, ID 271031. DOI: 10.1155/2013/271031.

[3] Miguel, L.F.F. and Fadel Miguel, L.F. (2012). Shape and Size Optimization of Truss Structures Considering Dynamic Constraints through Modern Metaheuristic Algorithms, Expert Systems with Applications 39(10), pp. 9458-9467. DOI: 10.1016/j.eswa.2012.02.113.

[4] Tejani, G.G., Savsani, V.J., Patel, V.K. and Mirjalili, S. (2018). Truss optimization with natural frequency bounds using improved symbiotic organisms search, Knowledge-Based Systems, 143, pp. 162–178. DOI: 0.1016/j.knosys.2017.12.012.

[5] Zakian, P. (2019). Meta-heuristic design optimization of steel moment resisting frames subjected to natural frequency constraints, Advances in Engineering Software, 135. DOI: 10.1016/j.advengsoft.2019.102686.

[6] Nguyen-Van, S., Nguyen, K.T., Luong, V.H., Lee, S. and Lieu, Q.X. (2021). A novel hybrid differential evolution and symbiotic organisms search algorithm for size and shape optimization of truss structures under multiple frequency constraints, Expert Systems with Applications, 184. DOI: 10.1016/j.eswa.2021.115534.

[7] Lemonge, A.C.C., Carvalho, J.P.G., Hallak, P.H. and Vargas, D.E.C. (2021). Multi-objective truss structural optimization considering natural frequencies of vibration and global stability, Expert Systems with Applications 165. DOI: 10.1016/j.eswa.2020.113777.

[8] Yang, G. (2001). Large-scale magnetorheological fluid damper for vibration mitigation: modeling, testing and control, Ph.D. Thesis, University of Notre Dame, USA.

[9] Dyke, S.J. (1996). Acceleration feedback control strategies for active and semi-active control systems - modeling, algorithm development, and experimental verification, Ph.D. Thesis, University of Notre Dame, USA.

[10] Dyke, S.J., Spencer Jr B.F., Sain, M.K. and Carlson, J.D. (1998). An Experimental Study of MR Dampers for Seismic Protection, Smart Materials and Structures 7(5), pp. 693-703. DOI: 10.1088/0964-1726/7/5/012.
[11] Yi, F., Dyke, S.J., Caicedo, J.M. and Carlson, J.D. (2001). Experimental Verification of Multi-Input Seismic Control Strategies for Smart Dampers, ASCE Journal of Engineering Mechanics, 127 (11), pp.1152-1164. DOI: 10.1061/(ASCE)0733-9399(2001)127:11(1152).
[12] Xu, Z.D. and Shen, Y.P. (2003). Intelligent Bi-state Control for the Structure with Magnetorheological Dampers, Journal of Intelligent Material Systems and Structures 14(1), pp. 35-42. DOI: 10.1177/1045389X03014001004.
[13] Zhaodong, X. and Yingqing, G. (2008). Integrated intelligent control analysis on semi-active structures by using magnetorheological dampers, Science in China Series E: Technological Sciences 51(12), pp. 2280-2294.
[14] Kori, J.G. and Jangid, R.S. (2009). Semi-active MR dampers for seismic control of structures, Bulletin of the New Zealand Society for Earthquake Engineering 42(3), pp. 157-166. DOI: 10.5459/bnzsee.42.3.157-166.
[15] Bitaraf, M. and Hurlebaus, S. (2013). Semi-active adaptive control of seismically excited 20-story nonlinear building, Engineering Structures 56, pp. 2107–2118. DOI: 10.1016/j.engstruct.2013.08.031.
[16] Zhu, W.Q., Luo, M. and Dong, L. (2004). Semi-active control of wind excited building structures using MR/ER dampers, Probabilistic Engineering Mechanics 19(3), pp. 279-285. DOI: 10.1016/j.probengmech.2004.02.011.
[17] Xiangjun, Q., Xun'an, Z. and Cherry, S. (2008). Study on semi-active control of mega-sub- controlled structure by MR damper subject to random wind loads, Earthquake engineering and engineering vibration 7, pp. 285-294. DOI: 10.1007/s11803-008-0838-3.
[18] Askari, M., Li J. and Samali, B. (2011). Semi-active LQG control of seismically excited nonlinear buildings using optimal Takagi-Sugeno inverse model of MR dampers, Procedia Engineering 14, pp. 2765–2772. DOI: 10.1016/j.proeng.2011.07.348.
[19] Brandão, F. da S. and Miguel, L.F.F. (2023). A New Methodology for Optimal Design of Hybrid Vibration Control Systems (MR+TMD) for Buildings under Seismic Excitation, Shock and Vibration, Volume 2023, Article ID 8159716,. DOI: 10.1155/2023/8159716.
[20] Chen, Z.Q., Wang ,X.Y., Ko, J.M., Ni, Y.Q., Spencer Jr, B.F., Yang, G. and Hu, J.H. (2004). MR damping system for mitigating wind-rain induced vibration on Dongting Lake Cable-Stayed Bridge, Wind and Structures 7(5), pp. 293-304. DOI: 10.12989/was.2004.7.5.293.
[21] César, M.T.B. (2015). Vibration Control of Building Structures using MagnetoRheological Dampers, Ph.D. Thesis, FEUP, Portugal.
[22] Miguel, L.F.F., Fadel Miguel, L.F., and Lopez, R.H. (2014). Robust design optimization of friction dampers for structural response control, Structural Control and Health Monitoring 21(9), pp. 1240-1251. DOI: doi.org/10.1002/stc.1642.
[23] Miguel, L.F.F., Fadel Miguel, L.F., and Lopez, R.H. (2015). A firefly algorithm for the design of force and placement of friction dampers for control of man-induced vibrations in footbridges, Optimization and Engineering 16, pp. 633-661. DOI: 10.1007/s11081-014-9269-3.
[24] Miguel, L.F.F., Fadel Miguel, L.F., and Lopez, R.H. (2016a). Simultaneous optimization of force and placement of friction dampers under seismic loading, Engineering Optimization 48(4), pp. 582-602. DOI: 10.1080/0305215X.2015.1025774
[25] Miguel, L.F.F., Fadel Miguel, L.F., and Lopez, R.H. (2016b). Failure probability minimization of buildings through passive friction dampers, The Structural Design of Tall and Special Buildings 25(17), 2016b, pp. 869-885. DOI: doi.org/10.1002/tal.1287.
[26] Miguel, L.F.F., Fadel Miguel, L.F., and Lopez, R.H. (2018). Methodology for the simultaneous optimization of location and parameters of friction dampers in the frequency domain, Engineering Optimization 50(12), pp. 2108-2122. DOI: 10.1080/0305215X.2018.1428318.
[27] Fadel Miguel, L.F., Lopez, R.H., and Miguel, L.F.F. (2013). Discussion of paper: Estimating optimum parameters of tuned mass dampers using harmony search [Eng. Struct. 33 (9) (2011) 2716-2723], Engineering Structures, 54, pp. 262-264, DOI: 10.1016/j.engstruct.2013.03.042.
[28] Miguel, L.F.F., and Santos, G.P. (2021). Optimization of multiple tuned mass dampers for road bridges taking into account bridge-vehicle interaction, random pavement roughness, and uncertainties", Shock and Vibration. 6620427, pp. 1-17. DOI: 10.1155/2021/6620427.
[29] Fadel Miguel, L.F., Lopez, R.H., Miguel, L.F.F., and Torii, A.J. (2016a). A novel approach to the optimum design of MTMDs under seismic excitations, Structural Control and Health Monitoring 23(11), pp. 1290-1313. DOI: 10.1002/stc.1845.
[30] Fadel Miguel, L.F., Lopez, R.H., Torii, A.J., Miguel, L.F.F., and Beck, A.T. (2016b). Robust design optimization of TMDs in vehicle–bridge coupled vibration problems, Engineering Structures 126, pp.703-711. DOI: 10.1016/j.engstruct.2016.08.033

[31] Ontiveros-Pérez, S.P., Miguel, L.F.F., and Fadel Miguel, L.F. (2017a). Optimization of location and forces of friction dampers, REM - International Engineering Journal 70(3), pp. 273-279. DOI: 10.1590/0370-44672015700065.
[32] Ontiveros-Pérez, S.P., Miguel, L.F.F., and Fadel Miguel, L.F. (2017b). Robust simultaneous optimization of friction damper for the passive vibration control in a Colombian building, Procedia Engineering 199, pp. 1743-1748. DOI: 10.1016/j.proeng.2017.09.430.
[33] Ontiveros-Pérez, S.P., Miguel L.F.F., and Fadel Miguel, L.F. (2017c). A new assessment in the simultaneous optimization of friction dampers in plane and spatial civil structures, Mathematical Problems in Engineering 2017(6040986), pp.1-18. DOI: 10.1155/2017/6040986.
[34] Ontiveros-Pérez, S.P., Miguel, L.F.F., and Riera, J.D. (2019). Reliability-based optimum design of passive friction dampers in buildings in seismic regions, Engineering Structures 190, pp. 276-284. DOI: 10.1016/j.engstruct.2019.04.021.
[35] Ontiveros-Pérez, S.P., and Miguel, L.F.F. (2022). Reliability-based optimum design of multiple tuned mass dampers for minimization of the probability of failure of buildings under earthquakes, Structures 42, pp. 144-159. DOI: 10.1016/j.istruc.2022.06.015.
[36] Vellar, L.S., Ontiveros-Pérez, S.P., Miguel, L.F.F., and Fadel Miguel, L.F. (2019). Robust optimum design of multiple tuned mass dampers for vibration control in buildings subjected to seismic excitation, Shock and Vibration 2019(9273714), pp. 1-9. DOI: 10.1155/2019/9273714.
[37] Brandão, F. da S., and Miguel, L.F.F. (2020). Vibration control in buildings under seismic excitation using optimized tuned mass dampers, Frattura ed Integrità Strutturale 14(54), pp. 66-87. DOI: 10.3221/IGF-ESIS.54.05.
[38] Brandão, F. da S., Almeida, A.K., and Miguel, L.F.F. (2022). Optimum design of single and multiple tuned mass dampers for vibration control in buildings under seismic excitation, International Journal of Structural Stability and Dynamics 2250078. DOI: 10.1142/S021945542250078X.
[39] Rossato, B.B., and Miguel, L.F.F. (2023). Robust optimum design of tuned mass dampers for high-rise buildings subject to wind-induced vibration, Numerical Algebra, Control & Optimization, 13, pp. 154-168, DOI: 10.3934/naco.2021060.
[40] Brito, J.W.S., Miguel, L.F.F. (2022). Optimization of a reinforced concrete structure subjected to dynamic wind action, Frattura ed Integrità Strutturale, 16, pp. 326-343, DOI: 10.3221/IGF-ESIS.59.22.
[41] Henao-Leon, D., Miguel, L.F.F.; and Villalba-Morales, J.D. (2023). A proposal for the optimization of the geometric configuration of a hollow cylindrical steel damper with slots, Journal of the Brazilian Society of Mechanical Sciences and Engineering, 45, 152, DOI: 10.1007/s40430-022-03919-8.
[42] Miguel, L.F.F., and Souza, O.A.P. (2023). Robust optimum design of MTMD for control of footbridges subjected to human-induced vibrations via the CIOA, Structural Engineering and Mechanics, 86, pp. 647-661. DOI: 10.12989/sem.2023.86.5.647.
[43] ASCE. (2016). Minimum Design Loads and Associated Criterion for Buildings and Other Structures, SEI: 7-16, 2016.
[44] Bachmann, H. (1995). Vibration Problems in Structures: Practical Guidelines. Berlin, Birkhauser.
[45] Marcadella, C. and Alberti, F.A. (2017). Comparative analysis of horizontal displacements of three structural bracing systems subjected to static wind loads influence, Proceedings of the 59th Brazilian Concrete Congress.
[46] Almeida, A.K. and Miguel, L.F.F. (2021). Structural Optimization and Vibration Control using Magneto-Rheological Dampers in Tall Buildings under Dynamic Wind Load, Proceedings of the XLII Ibero-Latin-American Congress on Computational Methods in Engineering.
[47] Clough, R.W. and Penzien, J. (1995). Dynamics of Structures, Berkeley, Computers & Structures Inc.
[48] ABNT. (1988). Forças devidas ao vento em edificações, NBR: 6123, 1988.
[49] Da Silva, N.P., and Miguel, L.F.F. (2023). Methodology for simulation of combined EPS and TS wind field and its influence on the dynamic response of a transmission line segment", International Journal of Structural Stability and Dynamics, 23(6), 2350058. DOI: 10.1142/S021945542350058X.
[50] Shinozuka, M. and Jan, C.M. (1972). Digital simulation of random processes and its applications, Journal of Sound and Vibration 25(1), pp. 111-128.
[51] Blessmann, J. (1995). O vento na Engenharia Estrutural, Brasil, Editora da UFRGS.
[52] Miguel, L.F.F., Fadel Miguel, L.F., Riera, J.D., Kaminski Jr., J. and Menezes, R.C.R. (2012). Assessment of code recommendations through simulation of EPS wind loads along a segment of a transmission line, Engineering Structures 43, pp. 1-11. DOI: 10.1016/j.engstruct.2012.05.004.
[53] Riera, J.D. and Ambrosini, R.D. (1992). Analysis of structures subjected to random loading using the transfer matrix or numerical integration methods, Engineering Structures, 14(3), pp.176-179. DOI: 10.1016/0141-0296(92)90028-O.
[54] Symans, M.D. and Constantinou, M.C. (1999). Semi-active control systems for seismic protection of structures: a state-of-the-art review, Engineering Structures 21(6), pp. 469-487. DOI: 10.1016/S0141-0296(97)00225-3.

[55] Spencer Jr, B.F., Dyke, S.J., Sain, M.K. and Carlson, J.D. (1997). Phenomenological Model of a Magnetorheological Damper, ASCE Journal of Engineering Mechanics 123(3), pp. 230-253. DOI: 10.1061/(ASCE)0733-9399(1997)123:3(230).
[56] Spencer Jr, B.F. and Sain, M.K. (1997). Controlling Buildings: A New Frontier in Feedback, IEEE Control Systems Magazine on Emerging Technology 17(6), pp. 19–35. DOI: 10.1109/37.642972.
[57] Rao, S.S. (2011). Mechanical Vibrations, USA, Pearson Prentice Hall.
[58] Soong, T.T. (1990). Active Structural Control: Theory and Practice, New York, John Wiley & Sons.
[59] Meirovitch, L. (1990). Dynamics and control of structures, New York, John Wiley & Sons.
[60] Wang, Y. (2006). Control strategies for 3d smart base isolation systems using modal and nodal approaches, Ph.D. Thesis, Washington University, USA.
[61] Ogata, K. (2010). Modern Control Engineering, USA, Pearson Education.
[62] Carneiro, R.B. (2009). Controle Semi-Ativo De Vibrações Em Estruturas Utilizando Amortecedor Magnetorreológico, PhD Thesis, Universidade de Brasília, Brasil.